IEEE Access

Received August 2, 2019, accepted September 5, 2019, date of publication October 1, 2019, date of current version November 8, 2019.

Digital Object Identifier 10.1109/ACCESS.2019.2944898

Decentralized Unified Control for Inverter-Based AC Microgrids Subject to Voltage Constraints

RICARDO PÉREZ-IBACACHE[1], AMIRNASER YAZDANI[2], (Senior Member, IEEE), CÉSAR SILVA[3], (Member, IEEE), AND JUAN C. AGÜERO[3], (Member, IEEE)

[1]Escola Politécnica, Pontifícia Universidade Católica do Rio Grande do Sul, Porto Alegre 90619-900, Brazil
[2]Department of Electrical and Computer Engineering, Ryerson University, Toronto, ON M5B 2K3, Canada
[3]Department of Electronic Engineering, Universidad Técnica Federico Santa María, Valparaíso 2390123, Chile

Corresponding author: Ricardo Pérez-Ibacache (ribacache@pucrs.br)

This work was supported in part by the Coordenação de Aperfeiçoamento de Pessoal de Nível Superior—Brasil (CAPES)—Finance Code 001, in part by CONICYT, Chile, under Grant 21141205, in part by the Chilean National Commission for Scientific and Technological Research, Fondecyt, under Grant 1181158, and in part by the CONICYT-Basal Project under Grant FB0821 (CCTVal) and Grant FB0008 (AC3E).

ABSTRACT The control law of electronically-interfaced distributed energy resources (DERs) must be able to maintain the stability and voltage regulation of the host microgrid in the two modes of operation. Ideally, this should be achieved by a decentralized primary control strategy that is independent of any communication infrastructure in order to increase the resilience of the microgrid. This is challenging as the primary control objectives in islanded and grid-connected modes of operation are conflicting. This paper proposes a decentralized control law for DER units based on state feedback and disturbance rejection. The controller provides an integral action which enables output current reference tracking. An ad-hoc partial input saturation technique is also proposed in order to prevent the integral action from having an adverse impact on the voltage amplitude and frequency regulation in the islanded mode of operation. The effectiveness of the proposed control strategy is demonstrated via a time-domain simulation of a medium-voltage distribution network with three embedded DER units, as well as through an experimental three-bus microgrid with two DER units. The results demonstrate the robustness of the proposed control strategy to transitions between the modes of operation and other network topological changes.

INDEX TERMS Complex oscillator network, decentralized primary control, input saturation, microgrid mode of operation, power sharing, robustness, seamless transition.

I. INTRODUCTION

The widespread deployment of microgrids with distributed energy resources (DERs) can reduce energy costs and enhance power system's resilience to extreme events [1]. However, several technical challenges need to be overcome in order to achieve the benefits of microgrids [2], [3]. In particular, in the islanded mode of operation, the microgrid's voltage amplitude and frequency must be stabilized and regulated by the DER units themselves (this function is often referred to as grid-forming or grid-supporting), whereas in the grid-connected mode the DER units are controlled as current sources (grid-feeding) [4], [5]. Since the modern power systems are subject to diverse and numerous disturbances, the DER units should be able to transition between the aforementioned conflicting control objectives. The stability of the microgrid can be compromised as a consequence of these transitions [1], [6]. The main goal of this paper is to develop a decentralized primary control law that ensures smooth transitions between the DER units' control objectives in the two modes of operation and continuous operation of the microgrid.

Most of the published work in the literature propose switching between different control strategies and rely upon islanding detection algorithms, [7]–[13]. However, such changes of control depend heavily on the accuracy of the islanding detection algorithm. Furthermore, dynamic transitions between controllers may lead to undesirable discontinuities. Consequently, the stability and performance robustness of the DER units operating in a closed loop may be adversely affected, as discussed in [14]. Some publications propose a single control for the microgrid, [15]–[18]. These publications focus on either providing current tracking

The associate editor coordinating the review of this manuscript and approving it for publication was Auday A.H. Mohamad.

in the grid-connected mode, or voltage regulation in the islanded mode. In addition, some of these proposals are dependent on external or centralized commands, which they receive via communications infrastructure, for synchronization purposes or for control, and therefore they are not fully decentralized. On the other hand, a decentralized control termed *unified DER control* has been proposed in [19], [20]. The proposal uses a controller that offers integral action with saturation, in order to change the control objective in response to a change in the microgrid's mode of operation. The proposed unified control successfully tracks the active and reactive power references in the grid-connected mode, and achieves the desired voltage amplitude and frequency regulation in the islanded mode. Both works assume decoupled active and reactive powers, and hence conventional droop-based control based on single-input single-output control design is used. However, in distribution power networks, the active and reactive powers are not decoupled, as highlighted in [6] and [21]. Thus, the performance of the closed-loop control can be poor. An alternative for dealing with the active and reactive power coupling is proposed in [22], where a linear optimal multivariable framework is used to provide stability and performance robustness to the DER-microgrid interaction.

In the current work, we propose a multivariable feedback law that is designed based on a linearized equivalent lumped dynamic model of the DER-microgrid interaction presented in [22]. However, the model is extended to also include a disturbance model. The disturbance signal represents not only the unmodeled dynamics of the microgrid but also the modeling errors caused by the linearization. The well-known solution to the linear quadratic Gaussian (LQG) control problem is adopted as the control strategy for each DER unit, and the control consists of a state feedback gain applied to the estimated states. In this proposal, the disturbance is estimated along with the state, and it is compensated in the control to realize integral action in the closed loop. Thus, output current tracking in the grid-connected mode is achieved. In the attempt to achieve current tracking, the regulation of voltage amplitude and frequency at each DER unit's point of connection (PoC) in the islanded mode of operation may be adversely affected. To counteract the possible adverse effect of the integral action, this work builds upon the ideas presented in [19] and [20], proposing a multivariable controller with a partial saturation of the input voltage amplitude and frequency. In this mode of operation, the feedback gain path is preserved and acts as a multivariable droop. Thus, a single multivariable unified control law, which achieves current tracking in the grid connected mode and voltage and frequency regulation in the islanded mode, is derived for the DER units. To do so, several features of the previous unified control proposals have been formulated within a multivariable framework using modern control and estimation techniques. The effectiveness of the proposed unified control is demonstrated through time-domain simulation of a test microgrid based on a medium-voltage distribution network [23] in the PSCAD/EMTDC software environment, as well as through an experimental three-bus microgrid with two DER units.

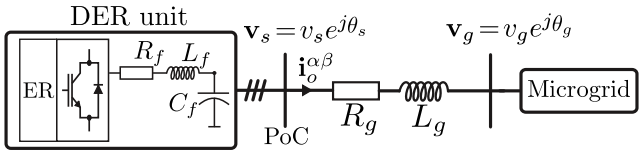

FIGURE 1. Schematic diagram of the DER-microgrid interaction.

II. DER-MICROGRID DISTURBANCE MODEL

A. SIMPLIFIED DISTURBANCE MODEL FOR DER-MICROGRID DYNAMICS

A DER unit consists of a primary energy resource (ER) and its grid interface power converter. The DER units are connected to the loads through a network of transformers and distribution lines to form a local power system or microgrid [24]. The interaction between a DER unit and the microgrid can be represented approximately by a simplified lumped model [22], which can be used to design a multivariable stabilizing controller for DER unit. In the current paper, we extend the control presented in [22] to also include output current reference tracking. To that end, the uncertainties of the nominal model are identified as input disturbances, which are estimated, and compensated for, so as to achieve integral action. Given that the microgrid can be tied to or islanded from a larger host electric power system, this paper assumes that the grid voltage is an uncertainty of the nominal model.

A simplified three-phase representation of a DER unit and its interaction with a microgrid can be obtained by the two bus model presented in Fig. 1. Here, one bus voltage is assumed to be imposed by the DER unit $v_s e^{j\theta_s}$, while the inner bus represents the uncertain grid voltage $v_g e^{j\theta_g}$. The parameters of the lumped model are R_g and L_g, and it is assumed that they are dominated by the short circuit parameters of the isolation transformer. This means that the control design of each DER unit only requires local knowledge of the values of resistance and leakage inductance of its own isolation transformer. Any mismatch between the transformer parameter and the total series equivalent impedance will be condensed in the input disturbance model. A load angle $\delta = \theta_g - \theta_s$ can be defined, where $\omega_g = \frac{d\theta_g}{dt}$ and $\omega_s = \frac{d\theta_s}{dt}$. The circuit model of Fig. 1, expressed on a stationary $\alpha - \beta$ frame, can be represented in a synchronous reference $d - q$ frame aligned with the voltage $\mathbf{v}_s$ at the respective PoC of each DER unit as:

$$L_g \frac{\mathbf{d}\mathbf{i}_o}{\mathbf{d}t} = -R_g \mathbf{i}_o - j\omega_s L_g \mathbf{i}_o - v_g e^{j\delta} + v_s, \tag{1}$$

$$\frac{d\delta}{dt} = \omega_g - \omega_s. \tag{2}$$

The lumped model above assumes that the voltage $\mathbf{v}_s$ of the DER unit's output filter appears to the network as an ideal voltage source (in other words, the dynamics of the $\mathbf{v}_s$ voltage-control loops are ignored for model reduction

purposes). The inner loop controlling $\mathbf{v}_s$ is designed for a bandwidth of about 1500 $[rad/s]$ for the DER unit and, as will be seen later, it is faster than the outer loop of interest in this work. This model reduction approach has been suggested in [25], [26], and others, but it has also been criticized in [5]. In this paper, we design a control strategy that minimizes the impact of the resulting modeling error (due to model reduction) on the performance of the control loop.

To formalize the aforementioned model, let us express (1) and (2) in a state-space form:

$$\dot{\mathbf{x}} = \mathbf{f}(\mathbf{x}) + \mathbf{g}(\mathbf{x})\mathbf{u} + \mathbf{p}(\mathbf{x})\mathbf{d}, \tag{3}$$

$$\mathbf{y} = \mathbf{C}\mathbf{x}, \tag{4}$$

$$\mathbf{f}(\cdot) = \begin{bmatrix} -\frac{R_g}{L_g}x^{(1)} \\ -\frac{R_g}{L_g}x^{(2)} \\ 0 \end{bmatrix}, \quad \mathbf{g}(\cdot) = \begin{bmatrix} \frac{1}{L_g} & x^{(2)} \\ 0 & -x^{(1)} \\ 0 & -1 \end{bmatrix},$$

$$\mathbf{p}(\cdot) = \begin{bmatrix} -\frac{\cos x^{(3)}}{L_g} & 0 \\ -\frac{\sin x^{(3)}}{L_g} & 0 \\ 0 & 1 \end{bmatrix}, \tag{5}$$

where the variable $x^{(j)}$ corresponds to the j-th element of the state vector $\mathbf{x} = \begin{bmatrix} i_{od} & i_{oq} & \delta \end{bmatrix}^T$, and the input $\mathbf{u}$ embeds the voltage amplitude and frequency at the DER unit's PoC, i.e., $\mathbf{u} = \begin{bmatrix} v_s & \omega_s \end{bmatrix}^T$. The disturbances in this model are the voltage amplitude and frequency of the microgrid's lumped dynamic model, that is, $\mathbf{d} = \begin{bmatrix} v_g & \omega_g \end{bmatrix}^T$. Certainly, since a decentralized control law is to be found, $\mathbf{d}$ cannot be measured or controlled. However, it is possible to estimate it and to compensate for it in the control loop as will be discussed in the next section. Finally, since current $\mathbf{i}_o$ defines the operating point of the DER unit, it is the output variable to be controlled, $\mathbf{y} = \begin{bmatrix} i_{od} & i_{oq} \end{bmatrix}^T$. The setpoint $\mathbf{y}_{ref}$ is typically given by a maximum power point tracking algorithm for the renewable energy resources, or by an energy management system for dispatchable resources. The formulation and design of the proposed control are based on a linearized discrete-time version of (3), which is obtained in the next section.

B. LINEARIZED DISCRETE-TIME MODEL

The tuning and implementation of the proposed control requires a linear representation of model (3). For the purpose of linearization, the state equilibrium point $\mathbf{x_0} = \begin{bmatrix} 0 & 0 & 0 \end{bmatrix}^T$ and the input and disturbance operating point $\mathbf{u_0} = \mathbf{d_0} = \begin{bmatrix} v_\mathbf{b} & \omega_\mathbf{b} \end{bmatrix}^T$ are chosen. Then, the linearized model becomes

$$\dot{\mathbf{x}} = \mathbf{A}\mathbf{x} + \mathbf{B}\mathbf{u} + \mathbf{P}\mathbf{d}, \quad \mathbf{y} = \mathbf{C}\mathbf{x}, \tag{6}$$

$$\mathbf{A} = \frac{\partial \{\mathbf{f}(\mathbf{x}) + \mathbf{g}(\mathbf{x})\mathbf{u} + \mathbf{p}(\mathbf{x})\mathbf{d}\}}{\partial \mathbf{x}}\Big|_{o.p.} = \begin{bmatrix} -\frac{R_g}{L_g} & \omega_\mathbf{b} & 0 \\ -\omega_\mathbf{b} & -\frac{R_g}{L_g} & -\frac{v_\mathbf{b}}{L_g} \\ 0 & 0 & 0 \end{bmatrix}, \tag{7}$$

$$\mathbf{B} = \mathbf{g}(\mathbf{x_0}) = \begin{bmatrix} \frac{1}{L_g} & 0 \\ 0 & 0 \\ 0 & -1 \end{bmatrix}, \quad \mathbf{P} = \mathbf{p}(\mathbf{x_0}) = -\mathbf{B},$$

$$\mathbf{C} = \begin{bmatrix} \mathbb{I}_2 & \mathbf{0} \end{bmatrix}, \tag{8}$$

where "$o.p.$" signifies evaluation at the operating point.

Assuming that $\mathbf{u}(t)$ and $\mathbf{d}(t)$ are deterministic constant signals between two consecutive sampling instants with values $\mathbf{u}_k$ and $\mathbf{d}_k$, the following discrete-time state-space representation is obtained

$$\mathbf{x}_{k+1} = \mathbf{A_d}\mathbf{x}_k + \mathbf{B_d}\mathbf{u}_k + \mathbf{P_d}\mathbf{d}_k, \quad \mathbf{y}_k = \mathbf{C_d}\mathbf{x}_k, \tag{9}$$

$$\mathbf{A_d} = \mathbf{e}^{T_s\mathbf{A}}, \quad \mathbf{B_d} = -\mathbf{P_d} = \int_0^{T_s} \mathbf{e}^{\mathbf{A}\tau}\mathbf{B}d\tau, \ \mathbf{C_d} = \mathbf{C}, \tag{10}$$

where T_s is the sampling period.

The model (9)-(10) describes the interactions of the DER unit with the rest of the microgrid over a wide range of possible operating conditions. It should be noted that variable $\mathbf{d}_k$, in addition to modeling the effects of the microgrid topological changes and parametric mismatches, also embeds other sources of uncertainties such as demand changes. Therefore, a key task in the proposed control strategy is to estimate $\mathbf{d}_k$, as will be discussed in Section III.

III. PROPOSED CONTROL STRATEGY

In this section, the proposed decentralized control is presented; it uses a structure based on state feedback and disturbance compensation. For that purpose, the solution of the linear quadratic Gaussian (LQG) control problem is used to deal with the current reference tracking of the DER unit. LQG control is a well-known linear control method, that is well suited for the linearized model discussed in the previous section. This paper adopts the LQG formulation presented in [27] and [28] that includes disturbance estimation and compensation. This technique implements integral action in the controller, and achieves output current reference tracking, in spite of low-frequency uncertainties such as parameter mismatches. Nevertheless, under certain operating conditions, such as the islanded mode of operation, current tracking may require a voltage amplitude or frequency that is outside of the allowable regulation boundaries. For such cases, partial saturation of the input is proposed. Such partial saturation ensures a state feedback path and provides a stable saturated condition and smooth transition between the modes of operation.

A. LINEAR-QUADRATIC-GAUSSIAN CONTROL LAW

The LQG control requires estimates of state $\mathbf{x}_k$ and disturbance $\mathbf{d}_k$; therefore, a state and disturbance observer is implemented based on the linear dynamic model (9), but including noise and an extension of the state to incorporate diturbance $\mathbf{d}_k$, assuming that the disturbance exhibits slow variations. This leads to the following stochastic model:

$$\begin{bmatrix} \mathbf{x}_{k+1} \\ \mathbf{d}_{k+1} \end{bmatrix} = \begin{bmatrix} \mathbf{A_d} & \mathbf{P_d} \\ \mathbf{0} & \mathbb{I} \end{bmatrix} \begin{bmatrix} \mathbf{x}_k \\ \mathbf{d}_k \end{bmatrix} + \begin{bmatrix} \mathbf{B_d} \\ \mathbf{0} \end{bmatrix} \mathbf{u}_k + \begin{bmatrix} \boldsymbol{\eta}_\mathbf{x} \\ \boldsymbol{\eta}_\mathbf{d} \end{bmatrix}_k \tag{11}$$

$$\mathbf{y}_k = \mathbf{C_d}\mathbf{x}_k + \mathbf{e}_k \tag{12}$$

where the variables $\{\boldsymbol{\eta}_\mathbf{x}, \boldsymbol{\eta}_\mathbf{d}, \mathbf{e}_k\}$ are assumed to be uncorrelated Gaussian white noise with covariance matrices $\{\mathbf{Q_x}, \mathbf{Q_d}, \mathbf{R_y}\}$,

$$\begin{bmatrix}\boldsymbol{\eta}_\mathbf{x}\\ \boldsymbol{\eta}_\mathbf{d}\end{bmatrix}_k \sim \mathcal{N}\left(\mathbf{0}, \begin{bmatrix}\mathbf{Q_x} & \mathbf{0}\\ \mathbf{0} & \mathbf{Q_d}\end{bmatrix}\right), \quad \mathbf{e}_k \sim \mathcal{N}\left(\mathbf{0}, \mathbf{R_y}\right). \tag{13}$$

To obtain the estimated state and disturbance, the solution of the time-invariant linear-quadratic-estimator problem [28] (or steady-state Kalman filter) is used, leading to the following observer:

$$\begin{bmatrix}\mathbf{x}_{k|k}\\ \mathbf{d}_{k|k}\end{bmatrix} = \begin{bmatrix}\mathbf{x}_{k|k-1}\\ \mathbf{d}_{k|k-1}\end{bmatrix} + \begin{bmatrix}\mathbf{L_x}\\ \mathbf{L_d}\end{bmatrix}\left(\mathbf{y}_k - \begin{bmatrix}\mathbf{C_d} & \mathbf{0}\end{bmatrix}\begin{bmatrix}\mathbf{x}_{k|k-1}\\ \mathbf{d}_{k|k-1}\end{bmatrix}\right), \tag{14}$$

where $\begin{bmatrix}\mathbf{L_x}^T & \mathbf{L_d}^T\end{bmatrix}^T$ is the time-invariant observer gain and $\begin{bmatrix}\mathbf{x}_{k|k-1}^T & \mathbf{d}_{k|k-1}^T\end{bmatrix}^T$ is the expected value of the state and disturbance prediction. This prediction is based on model (11) and can be expressed as,

$$\begin{bmatrix}\mathbf{x}_{k+1|k}\\ \mathbf{d}_{k+1|k}\end{bmatrix} = \begin{bmatrix}\mathbf{A_d} & \mathbf{P_d}\\ \mathbf{0} & \mathbb{I}\end{bmatrix}\begin{bmatrix}\mathbf{x}_{k|k}\\ \mathbf{d}_{k|k}\end{bmatrix} + \begin{bmatrix}\mathbf{B_d}\\ \mathbf{0}\end{bmatrix}\mathbf{u}_k. \tag{15}$$

Finally, the covariance matrices in (13) are used to adjust the observer performance. The LQG control also requires the incorporation of a state feedback gain. The combination of the two, the observer and feedback gains, constitutes the LQG control. To obtain the feedback gain, the solution of the time-invariant linear-quadratic-regulator problem, which is based on the linear model (9), is adopted.

As mentioned in Section II, the controlled variables are the output currents $\mathbf{y}_k = \begin{bmatrix}i_{od} & i_{oq}\end{bmatrix}^T$, while the input variables are the voltage amplitude v_s and frequency ω_s at the PoC of each DER unit. The LQG control law with disturbance compensation and output current reference $\mathbf{y}_{ref}$ can be expressed as

$$\mathbf{u}_k = -\mathbf{K_x}\mathbf{x}_{k|k} + \mathbf{H_d}\mathbf{d}_{k|k} + \mathbf{H_r}\mathbf{y}_{ref}, \tag{16}$$

where $\mathbf{K_x}$ is the static state feedback gain, $\mathbf{H_r}$ is a static matrix designed to provide unity gain from $\mathbf{y}_{ref}$ to $\mathbf{y}_k$, and $\mathbf{H_d}$ is a static gain that maps disturbance $\mathbf{d}_k$ from the nominal model (9) to the input of the closed-loop system. Following the methodology presented in [27] and [28], the static gain from the reference to the output is $\mathbf{C_d}(\mathbb{I} - \mathbf{A_d} + \mathbf{B_d}\mathbf{K_x})^{-1}\mathbf{B_d}$, and hence the value of $\mathbf{H_r}$ is

$$\mathbf{H_r} = \left[\mathbf{C_d}(\mathbb{I} - \mathbf{A_d} + \mathbf{B_d}\mathbf{K_x})^{-1}\mathbf{B_d}\right]^{-1}. \tag{17}$$

In a similar way one can determine the static gain that cancels the effect of $\mathbf{d}_k$ on the controlled variables $\mathbf{y}_k$. Thus, $\mathbf{H_d} = -\mathbf{H_r}\left[\mathbf{C_d}(\mathbb{I} - \mathbf{A_d} + \mathbf{B_d}\mathbf{K_x})^{-1}\mathbf{P_d}\right]$. Based on (8), $\mathbf{P_d} = -\mathbf{B_d}$ and therefore $\mathbf{H_d} = \mathbb{I}$. Consequently, the control law (16) can be expressed as

$$\mathbf{u}_k = -\begin{bmatrix}\mathbf{K_x} & -\mathbb{I}\end{bmatrix}\begin{bmatrix}\mathbf{x}_{k|k}^T & \mathbf{d}_{k|k}^T\end{bmatrix}^T + \mathbf{H_r}\mathbf{y}_{ref}. \tag{18}$$

Thus, by evaluating the state and disturbance observer at each sampling time, based on (14), (15) and (18), the LQG control is obtained. Note that, due to the time required to execute (14) and (18), in practice this controller is implemented with a one-sample delay. Ignoring this delay in the model results in some high-frequency modeling errors. The errors, however, are not significant due to the large phase margin of the designed nominal closed-loop system. Since normal operation of a microgrid requires voltage amplitude and frequency regulation, this paper proposes a suitable saturation for the input variable, as is detailed in the next section.

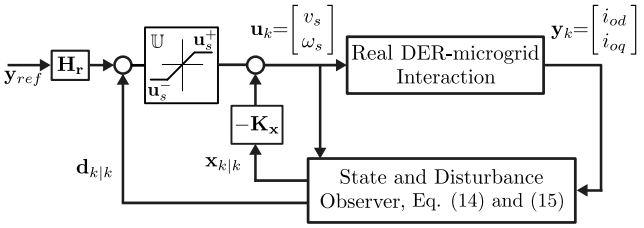

FIGURE 2. Scheme of the proposed LQG control with input saturation.

B. VOLTAGE AMPLITUDE AND FREQUENCY INPUT CONSTRAINTS

Since the proposed control law provides integral action, each DER unit within the microgrid attempts to adjust the voltage amplitude and frequency at its respective PoC to achieve output current reference tracking. However, this can lead the DER units to forbidden operating points in terms of voltage amplitude and frequency. Therefore, the control law (16) must be constrained without compromising the stability of the microgrid. Also, to ensure proper voltage amplitude and frequency regulation, and hence unified microgrid control, such a constraint in the input variable must be suitably implemented. Therefore, the proposed control corresponds to an LQG strategy with input saturation, schematized in Fig. 2.

In this paper, it is proposed that the stabilizing effect of the state feedback is retained regardless of the operating point or onset of saturation. Therefore, the control law (16) is modified to:

$$\mathbf{u}_k = -\mathbf{K_x}\mathbf{x}_{k|k} + \text{sat}\left\{\overline{\mathbf{u}}_k\right\}, \tag{19}$$

where

$$\overline{\mathbf{u}}_k = \mathbf{d}_{k|k} + \mathbf{H_r}\mathbf{y}_{ref} \tag{20}$$

and

$$\text{sat}\left\{\overline{u}_k^{(i)}\right\} \triangleq \begin{cases} u_s^{(i)+} & \text{if } \overline{u}_k^{(i)} \geq u_s^{(i)+}\\ \overline{u}_k^{(i)} & \text{if } u_s^{(i)-} \leq \overline{u}_k^{(i)} \leq u_s^{(i)+}\\ u_s^{(i)-} & \text{if } \overline{u}_k^{(i)} \leq u_s^{(i)-}. \end{cases} \tag{21}$$

In (21), $\overline{u}_k^{(i)}$ is the i-th element of $\overline{\mathbf{u}}_k$ in (20), and the values $u_s^{(i)+}$ and $u_s^{(i)-}$ define the permissible limits for $\overline{u}_k^{(i)}$. To formalize this bounded input, $\mathbb{U} \subset \mathbb{R}^2$ is defined as the delimited region for the variable sat$\{\overline{\mathbf{u}}_k\}$, such that $\mathbf{u}_s^- \leq \mathbb{U} \leq \mathbf{u}_s^+$. In addition, one can define the boundary of $\mathbb{U}$ as $\partial\mathbb{U} \in \mathbb{U}$. Then, if the nominal operating point of the DER unit is considered, the maximum deviation of the input can be

expressed as $\mathbf{u}_k = -\mathbf{K_x}\mathbf{x}_{nom} + \partial\mathbb{U}$. Consequently, $\mathbf{K_x}$ and $\partial\mathbb{U}$ can be determined so as to satisfy the maximum deviations specified in a given grid code, as will be discussed in the next subsection.

C. CLOSED LOOP SYSTEM PROPERTIES AND DESIGN

To assess the performance of the saturated LQG control for the DER-microgrid closed-loop dynamics, one can obtain the state-space representation from the output current reference $\mathbf{y}_{ref}$ to the actual output current $\mathbf{y}_k$, with the observer dynamics taken into account. To that end, (19) is modified to represent the input partial saturation in state-space form. The saturation is modeled by a diagonal matrix $\boldsymbol{\alpha}(t)$ as a variable that mimics the effect of saturation as $\text{sat}\{\overline{\mathbf{u}}_k\} = \boldsymbol{\alpha}(t)\overline{\mathbf{u}}_k$. Therefore, the control law (19) can be written as

$$\mathbf{u}_k = -\begin{bmatrix}\mathbf{K_x} & -\boldsymbol{\alpha}(t)\end{bmatrix}\begin{bmatrix}\mathbf{x}_{k|k}^T & \mathbf{d}_{k|k}^T\end{bmatrix}^T + \boldsymbol{\alpha}(t)\mathbf{H_r}\mathbf{y}_{ref}. \quad (22)$$

$$\overline{\mathbf{x}}_{k+1|k} = \overline{\mathbf{A}}_{cl}\overline{\mathbf{x}}_{k|k-1} + \overline{\mathbf{B}}_{cl}\mathbf{y}_{ref} + \overline{\mathbf{P}}_{cl}\mathbf{d}_k, \quad (23)$$

where the matrices $\{\overline{\mathbf{A}}_{cl}, \overline{\mathbf{B}}_{cl}, \overline{\mathbf{P}}_{cl}\}$ are defined in (24), as shown at the bottom of this page.

To obtain the closed-loop state-space representation, (14) and (22) are evaluated in (15), and (22) is evaluated in (9), finding $\{\mathbf{x}_{k+1|k}, \mathbf{d}_{k+1|k}\}$ and $\mathbf{x}_{k+1}$, respectively. In addition, it is beneficial to express the closed-loop state-space as a function of the state prediction error $\tilde{\mathbf{x}}_{k|k-1} = \mathbf{x}_k - \mathbf{x}_{k|k-1}$. Thus, one can define a new state-space vector that considers the system and controller as $\overline{\mathbf{x}}_{k|k-1} = \begin{bmatrix}\mathbf{x}_k^T & \tilde{\mathbf{x}}_{k|k-1}^T & \mathbf{d}_{k|k-1}^T\end{bmatrix}^T$, and the closed-loop state space can be written in the following form:

It should be noted that the eigenvalues of the block-diagonal transition matrix $\overline{\mathbf{A}}_{cl}$ do not depend on $\boldsymbol{\alpha}(t)$ and, thus, are constants. Therefore, the local stability about the operating point is assured by the gains $\{\mathbf{K_x}, \mathbf{L_x}, \mathbf{L_d}\}$ even when the control is partially saturated. In addition, the control offers an inherent anti-windup feature. If the observer, which is an active part of the control strategy, was fed by the output of the linear controller (equation (18)), instead of the actual plant input (equation (19)), the observer would suffer from a lack of information, and controller windup would occur. To avoid this, the observer based anti-windup strategy [29] is adopted in this work. It simply involves feeding the observer with the actual plant input. This condenses the effect of input nonlinearities in the state observer, and the closed-loop stability follows the analysis previously presented through variable $\boldsymbol{\alpha}(t)$. On the other hand, from the third rows of (23) and (24), it can be concluded that the prediction error reaches zero in steady state, which means that the feedback gain $-\mathbf{K_x}\mathbf{x}_{k|k}$ in (19) determines the deviation of voltage amplitude and frequency from their permissible limits imposed by the saturation. Finally, it is remarked that the feedback gain plays the role of a multivariable droop mechanism for all operating points, and therefore, power sharing criteria can be used for its design. To simplify the notation in the remaining section, for the study of the steady-state condition, the time-operator "k" is replaced with "∞".

1) STATE FEEDBACK GAIN DESIGN

As noted previously, the third rows of (23) and (24) imply that the prediction error is zero in steady state, $\tilde{\mathbf{x}}_{\infty|\infty} = \mathbf{0}$. In other words, the estimated state $\mathbf{x}_{k|k}$ converges to the actual values of currents $\{i_{od}, i_{oq}\}$ and angle δ in the DER-microgrid interaction model (9). Consequently, the state feedback gain $\mathbf{K_x}$ and the state of the system $\mathbf{x}_k$ are partly responsible for voltage amplitude and frequency regulation at the PoC of the DER unit, equation (19). Therefore, to bound its effect, $\mathbf{K_x}$ must be bounded such that at the nominal state operating point, the state feedback gain satisfies the following inequality:

$$-\Delta\mathbf{u}_f \leq \mathbf{K_x}\mathbf{x}_{nom} \leq \Delta\mathbf{u}_f. \quad (25)$$

The value of $\mathbf{x}_{nom}$ is obtained from the system model (6) as,

$$\mathbf{x}_{nom} = \begin{bmatrix} i_{od}^{nom} \\ i_{oq}^{nom} \\ \delta^{nom}\end{bmatrix} = \begin{bmatrix} I_n\cos\phi \\ I_n\sin\phi \\ -\dfrac{L_g}{v_b}(\omega_b I_n\cos\phi + \dfrac{R_g}{L_g}I_n\sin\phi)\end{bmatrix}, \quad (26)$$

where ϕ is the phase angle between voltage $\mathbf{v}_s$ and current $\mathbf{i}_o$ (power factor), i.e., $\phi \in [0, 2\pi]$, and $\{I_n, R_g, L_g\}$ are the nominal current and parameters for the DER unit. In (25), $\Delta\mathbf{u}_f$ may be defined by regulation standards, e.g., [30]. In this work, and for illustrative purposes, permissible variations of 2.5% for voltage amplitude and 0.5 Hz for voltage frequency are assumed, $\Delta\mathbf{u}_f = \begin{bmatrix}0.025v_b & \pi\end{bmatrix}^T$.

There is more than one $\mathbf{K_x}$ that satisfies inequality (25). This degree of freedom can be used to find a $\mathbf{K_x}$ that maximizes the DER-microgrid closed-loop robustness while (25) is satisfied. The solution to the LQR problem is adopted in this work due to its well-damped response and good robustness properties. LQR minimizes the cost function $J = \sum_{i=0}^{N=\infty}\mathbf{x}_i^T\Gamma_{\mathbf{x}}\mathbf{x}_i + \mathbf{u}_i^T\Omega_{\mathbf{u}}\mathbf{x}_i$ given the weighting factors $\Gamma_{\mathbf{x}}$ and $\Omega_{\mathbf{u}}$, so it is designed iteratively by adjusting these weighting factors to satisfy (25). Finally, as is seen from (23) and (24), the DER-microgrid closed-loop dynamic performance is not only a function of $\mathbf{K_x}$, but also a function

$$\overline{\mathbf{A}}_{cl} = \begin{bmatrix}\mathbf{A_d} - \mathbf{B_d}\mathbf{K_x} & \mathbf{B_d}\{\mathbf{K_x}(\mathbb{I} - \mathbf{L_x}\mathbf{C_d}) + \boldsymbol{\alpha}(t)\mathbf{L_d}\mathbf{C_d}\} & \mathbf{B_d}\boldsymbol{\alpha}(t) \\ \mathbf{0} & \mathbf{A_d}(\mathbb{I} - \mathbf{L_x}\mathbf{C_d}) + \mathbf{B_d}\mathbf{L_d}\mathbf{C_d} & \mathbf{B_d} \\ \mathbf{0} & \mathbf{L_d}\mathbf{C_d} & \mathbb{I}\end{bmatrix} \quad \overline{\mathbf{B}}_{cl} = \begin{bmatrix}\mathbf{B_d}\boldsymbol{\alpha}(t)\mathbf{H_r} \\ \mathbf{0} \\ \mathbf{0}\end{bmatrix} \quad \overline{\mathbf{P}}_{cl} = \begin{bmatrix}\mathbf{P_d} \\ \mathbf{P_d} \\ \mathbf{0}\end{bmatrix}. \quad (24)$$

of the observer gain $\left[\,\mathbf{L_x}^T\ \mathbf{L_d}^T\,\right]^T$. The design of the observer gain is addressed next.

2) STATE AND DISTURBANCE OBSERVER DESIGN

If (23) and (24) are evaluated in steady state, their second rows reveal that $\mathbf{B_d d}_{\infty|\infty} = -\mathbf{P_d d}_\infty$. This means that all the steady-state modeling errors condensed in $\mathbf{d}_\infty$ result to be estimated through the observer (14) in the variable $\mathbf{d}_{\infty|\infty}$. By evaluating this equality ($\mathbf{B_d d}_{\infty|\infty} = -\mathbf{P_d d}_\infty$) in the first row of (23), assuming non-saturated inputs ($\boldsymbol{\alpha}(t) = \mathbb{I}$), the effect of $\mathbf{d}_\infty$ is canceled out, $\mathbf{x}_\infty = (\mathbb{I} - \mathbf{A_d} + \mathbf{B_d K_x})^{-1}\mathbf{B_d H_r y}_{ref}$, and the output equation can be expressed as $\mathbf{y}_\infty = \mathbf{C_d}(\mathbb{I} - \mathbf{A_d} + \mathbf{B_d K_x})^{-1}\mathbf{B_d H_r y}_{ref}$. Through $\mathbf{H_r}$, (17), unity gain from the reference to the output is ensured. This clearly shows that the estimation and compensation of the disturbance $\mathbf{d}$ results in an integral action in the controller. Thus, provided that the voltage amplitude and frequency do not exceed the permissible boundaries, current reference tracking is achieved.

The aforementioned considerations take the steady-state operating point of the observer and feedback into account. The problems of stability and robustness are discussed next.

While the state feedback gain is obtained by solving the LQR problem with the weighting matrices $\Gamma_\mathbf{x}$ and $\Omega_\mathbf{u}$ subject to (25), the state observer gain is obtained by solving the LQE (or Kalman filter) problem with covariance matrices $\{\mathbf{Q_x}, \mathbf{Q_d}, \mathbf{R_y}\}$. To determine these parameters, the frequency response of the closed loop is examined during the design process. First, as the plant model has an eigenvalue at the origin and the controller has integral action, the return ratio presents a double integrator, thus giving rise to an unavoidable overshoot in the output tracking response. To minimize the overshoot, this paper considers a damping ratio $\xi \geq 0.7$ for each closed-loop mode. Second, the DER-microgrid interaction model presents a lightly-damped mode with a natural frequency of $\omega_b = 377\,[rad/s]$, as seen from (7). Therefore, to avoid the excitation of this mode, this paper considers a dominant closed-loop mode about $80\,[rad/s]$. On the other hand, the linearization errors, parameter mismatches, and load changes are considered low-frequency disturbances and within the attenuation band of the control ($80\,[rad/s]$). The design with these considerations is described in Section IV.

IV. SIMULATION RESULTS

The proposed control strategy is tested on a simulated microgrid based on the CIGRE benchmark for a North American three-phase medium-voltage (MV) distribution network [23]. Fig. 3 shows a single-line schematic diagram of the test microgrid, which is simulated in the PSCAD/EMTDC software environment. Two cases of practical interest are simulated in order to show the effectiveness of the proposed control. The first case shows that the output current tracks its reference if the voltage at the PoC of its respective DER unit is within the permissible boundaries. The second case

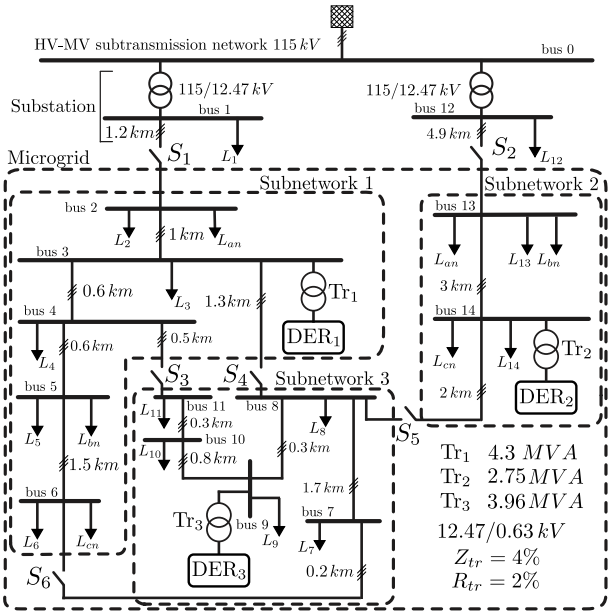

FIGURE 3. Schematic diagram of the CIGRE benchmark for a North American medium-voltage distribution network.

TABLE 1. Base values of the microgrid.

Base	Metric Value	Remark
S_b	11 [MVA]	base power
$V_{b\text{-}MV}$	$10.18\,[kV]$	base peak per-ph. Med. Volt.
$V_{b\text{-}LV}$	$0.52\,[kV]$	base peak per-ph Low Volt.
$I_{b\text{-}MV}$	$0.59\,[kA]$	$2S_b/(3V_{b\text{-}MV})$
$I_{b\text{-}LV}$	$14.1\,[kA]$	$2S_b/(3V_{b\text{-}LV})$
$Z_{b\text{-}LV}$	$36.9\,[m\Omega]$	$V_{b\text{-}LV}/I_{b\text{-}LV}$
ω_b	$377\,[rad/s]$	60-Hz nom-freq.
v_b	$0.52\,[kV]$	nom. Volt.
$V_{dc\text{-}b}$	$1.2\,[kV]$	base DC-link voltage.

demonstrates the ability of the control to adjust the output current to maintain the voltage within the tolerable range in the islanded mode, if the voltage at the PoC tends to fall outside of the permissible range.

The test microgrid can be energized by a $115\,kV/60\,Hz$ subtransmission line that is characterized by a short-circuit power of $S_{sc} = 5$ [GVA] and an R to X ratio of 0.1 (see Fig. 3). The microgrid is fed by two substation transformers with nominal powers of $S_{0\text{-}1} = 15$ [MVA] and $S_{0\text{-}12} = 12$ [MVA], and it can be divided into three subnetworks. It hosts three bidirectional dispatchable DER units, at buses 3, 14, and 9, which are interfaced by corresponding 12.47/0.63 [kV] transformers. Each DER unit is composed of a two-level VSC, a constant DC source v_{dc}, and an LC output filter. The VSCs are controlled by pulse-width modulation (PWM) whose switching frequency is selected to be the same as the sampling period for the control, T_s. The base values for the various quantities and the parameters of the DER units are presented in Tables 1 and 2, respectively. The natural frequencies and the damping ratios of the closed-loop eigenvalues for each DER unit are provided in Table 2. The

TABLE 2. DER Systems Circuit and Control Parameters.

Circuit Parameters (in per unit)				
Par.	DER_1	DER_2	DER_3	Remark
S_{nom}	0.39	0.25	0.36	–
R_f	0.023	0.036	0.025	$R_f/Z_{b\text{-}LV}$
L_f	0.179	0.280	0.194	$L_f\omega_b/Z_{b\text{-}LV}$
C_f	0.016	0.010	0.014	$C_f\omega_b Z_{b\text{-}LV}$
L_g	0.088	0.138	0.096	Ind. Lumped Mod.
R_g	0.051	0.080	0.056	Res. Lumped Mod.
v_{dc}	1.04			$v_{dc}/V_{b\text{-}dc}$
T_s	120 $[\mu s]$			Sampling Period
LQE and LQR Parameters				
$\mathbf{Q_x}$	$\text{diag}\{1,\ 1,\ 0.01\}$			State covariance
$\mathbf{Q_d}$	$\text{diag}\{5,\ 20\}$			Dist. covariance
$\mathbf{R_y}$	$\beta\times10^5\cdot\mathbb{I}_{2\times2}$			Meas. covariance
β	10	6	10	
$\mathbf{\Omega_x}$	$\mathbf{C_d}^T\mathbf{C_d}$			State weigh. factor
$\mathbf{\Gamma_u}$	$\gamma\times10^6\cdot\text{diag}\{0.02,1\}$			Input weigh. factor
γ	3	1.26	2.58	
Input Constraints for $\bar{\mathbf{u}}_k$				
$\mathbb{U}_1$	$\mathbf{u_s^{\pm}} = \begin{bmatrix} v_b(1\pm0.05) & \omega_b\pm\pi \end{bmatrix}^T$			
$\mathbb{U}_2$	$\mathbf{u_s^{\pm}} = \begin{bmatrix} v_b(1\pm0.025) & \omega_b\pm0.5\pi \end{bmatrix}^T$			
State Feedback design boundaries				
$\Delta\mathbf{u}_f$	$\begin{bmatrix} 0.025v_\mathbf{b} & \pi \end{bmatrix}^T$			$\mathbf{K_x}$ design, eq. (25)

Eigenvalues of the resulting closed-loop design

	$\lambda_{1,2}$		λ_3		$\lambda_{4,5}$		$\lambda_{6,7}$		λ_8	
	ω_n	ξ_n	ω_n	ξ_n	ω_n	ξ_n	ω_n	ξ_n	ω_n	ξ_n
DER_1	532	0.7	79	1	1476	0.7	3977	0.7	141	1
DER_2	533	0.7	80	1	1341	0.7	3614	0.7	141	1
DER_3	536	0.7	82	1	1417	0.7	3817	0.7	141	1

line parameters and nominal load powers for the network are specified in [23]. The static load models are in accordance with the system used in [23] (see also [22]).

The case studies presented here are designed to demonstrate the dynamic response of the DER units when the microgrid operates in the islanded mode and then transitions to grid-connected mode. The performance of the proposed control is demonstrated for two different sets of voltage and frequency boundaries, $\mathbb{U}_1$ and $\mathbb{U}_2$, which are listed in Table 2 and assumed to be the same for all DER units. The limit $\mathbb{U}_1$ is less restrictive than $\mathbb{U}_2$. Input constraints are determined such that, in the worst case, the input $\mathbf{u}_k$ does not go beyond $\pm7.5\%$ of the nominal voltage amplitude and $\pm2\pi$ $[rad/s]$ of the nominal frequency for $\mathbb{U}_1$, and $\pm5\%$ and $\pm\frac{3\pi}{2}$ $[rad/s]$ for $\mathbb{U}_2$. The resulting voltage amplitude and frequency deviations are due partly to the specified boundary $\mathbb{U}$ and partly to the effect of the stabilizing gain $\mathbf{K_x}$. In turn, $\mathbf{K_x}$ is determined through the procedure discussed in Section III-C.1 for a maximum deviation of 2.5 % of voltage amplitude and π $[rad/s]$ of voltage frequency. Finally, to solve the LQR problem, $\Omega_\mathbf{x}$ and $\Gamma_\mathbf{u}$ are chosen with the entries given in Table 2.

TABLE 3. Output current references (per unit).

	DER_1	DER_2	DER_3
$\mathbf{y}_{ref}$	$\begin{bmatrix}0.255 & -0.184\end{bmatrix}^T$	$\begin{bmatrix}0.142 & -0.085\end{bmatrix}^T$	$\begin{bmatrix}0.206 & -0.124\end{bmatrix}^T$

All the case studies under consideration involve the closure of some of the switches S_l (with $l \in \{1, ..., 6\}$), as labeled in Fig. 3. Even though synchronization may be implemented in practice, for these case studies the closure of switches takes place under nonzero switch voltages. This is done intentionally to test a severe disturbance to the microgrid and to demonstrate the robustness of the proposed control strategy.

In the results that follow, the output current magnitude $|\mathbf{i}_o| = \sqrt{i_{od}^2 + i_{oq}^2}$, the voltage magnitude at the PoC $|\mathbf{v}_s| = \sqrt{v_{sd}^2 + v_{sq}^2}$, and the frequency at the PoC ω_s, are expressed in per unit terms and plotted in black, blue, and red, for DER_1, DER_2, and DER_3, respectively. For the current magnitude waveforms, the dashed lines represent the output current references. It should be noted that the subnetworks are not entirely balanced and, consequently, oscillations at twice the fundamental frequency appear in some of the waveforms.

A. CASE 1: RESPONSE TO TOPOLOGICAL CHANGES OF THE ISLANDED NETWORK

This case study demonstrates the DER units' transient and steady-state responses under different operating conditions in the islanded mode. Initially, the microgrid's subnetworks all start in the islanded mode of operation, i.e., switches S_l (with $l \in \{1, .., 6\}$) are all open. Thus, each subnetwork is energized by its corresponding DER unit. The output current reference of each DER unit, $\mathbf{y}_{ref}$, is initially set to the values presented in Table 3. These references are different to the local current demand of the respective subnetwork. Therefore, the integral action of the control, which attempts to enforce these references, leads to the saturation of term $\bar{\mathbf{u}}_k$ in all DER units, while the state feedback actions $-\mathbf{K_x}\mathbf{x}_{k|k}$ stabilize the networks.

We next analyze two cases of interest at $t = 0.1\,s$ and $t = 0.4$. At $t = 0.1\,s$, while the voltages of bus 3 and bus 8 exhibit a phase difference of approximately 3°, switch S_4 is closed and connects subnetworks 1 and 3. As Fig. 4 shows, the first noticeable effect is that DER_1 and DER_3 change their frequencies transiently to synchronize with each other. It is also observed that the responses of the voltages, frequencies, and currents are well-damped with nearly the same dynamics as those predicted by the designed closed-loop dominant modes.

Table 4a lists the steady-state powers of the DER units after the closure of S_4. It can be seen that active and reactive powers are shared approximately in proportion to the respective DER

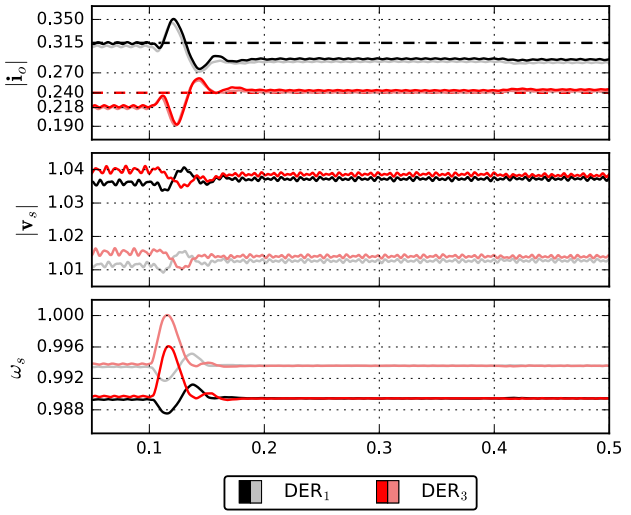

FIGURE 4. DER units 1 and 3 responses to the connection of the subnetworks 1 and 3 in the islanded mode of operation. Response for input constraint $\mathbb{U}_1$ in dark-color lines and for input constraint $\mathbb{U}_2$ in light-color lines.

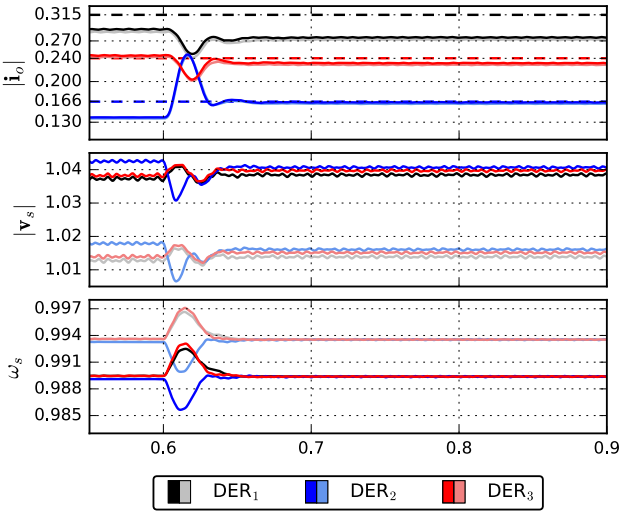

FIGURE 5. DER unit responses to the connection of the subnetwork 2 to the subnetworks 1 and 3 in islanded mode of operation. Response for input constraint $\mathbb{U}_1$ in dark-color lines and for input constraint $\mathbb{U}_2$ in light-color lines.

TABLE 4. DER unit's Delivered Power (per unit, base power of each DER).

DER$_1$		DER$_3$		DER$_1$		DER$_2$		DER$_3$	
P	Q	P	Q	P	Q	P	Q	P	Q
0.66	0.39	0.62	0.33	0.64	0.35	0.62	0.30	0.60	0.3

(a) Subnetworks 1 and 3. (b) Subnetworks 1, 2 and 3.

units' nominal powers, with a deviation from an exact shares of only 3%. Finally, at $t = 0.4\,s$, switches S_3 and S_6 are closed, changing the topology from radial to meshed without any major transient or steady-state effect, as shown in Fig. 4.

The response of the connection of subnetwork 2 to subnetworks 1 and 3 is shown in Fig. 5; the connection is accomplished by closing switch S_5 at $t = 0.6\,s$. Again, a phase displacement of 3° is allowed between the voltages of bus 8 and bus 14 before the closure of S_5. As in the previous case, the dynamic responses of the DER units correspond approximately to the designed closed-loop dominant modes, and, as can be seen in Table 4b, the powers are shared approximately proportional to the DER units' nominal powers with a deviation of only 3%.

For both aforementioned incidents, the integral action of the controller, manifested in term $\bar{\mathbf{u}}_k$, remains saturated at the upper bound of voltage amplitude and at the lower bound of voltage frequency, for both sets of input constraints $\mathbb{U}_1$ and $\mathbb{U}_2$ considered in this study. These results illustrate that the saturation of $\bar{\mathbf{u}}_k$ does not compromise the closed-loop stability, as also discussed in Section III-C.

B. CASE 2: TRANSITION TO GRID-CONNECTED MODE OF OPERATION

The second case study illustrates the transient and steady-state responses of the DER units to a transition to the grid-connected mode. To evaluate the ability of the proposed control strategy to regulate the microgrid's voltage, an amplitude deviation of -12% of the nominal voltage is intentionally allowed at bus 1 before the connection of switch S_1, while the voltage amplitude at bus 12 remains at nominal value. The microgrid is initially in a steady state with the switches S_3 through S_6 closed and switches S_1 and S_2 open, i.e. it is in the islanded mode of operation. Then, S_1 is closed at $t = 1.1\,s$, with the voltages of bus 1 and bus 2 having a phase displacement of about 3°, and S_2 is closed at $t = 1.5\,s$. The closure of S_1, connecting the microgrid to the host grid with a lower voltage, results in a reduction of voltages at the PoCs of the DER units, as shown in Fig. 6. Such a voltage reduction is handled differently depending on the limits, $\mathbb{U}_1$ or $\mathbb{U}_2$. As is illustrated in Fig. 8a, the term $\bar{\mathbf{u}}_k$ for the wider constraint $\mathbb{U}_1$ remains linear. Thus, the output currents of the DER units track their respective references. For the tighter constraint $\mathbb{U}_2$, however, $\bar{\mathbf{u}}_k$ crosses the boundary $\mathbb{U}_2$, and reaches a new steady-state with a saturated voltage amplitude at the lower boundary and an unsaturated frequency, as can be seen in Figs. 8a and 8b. Consequently, the control does not track the output current reference; instead, it counteracts the grid's voltage deviation by supplying the currents needed to keep the voltage at the lower bound of the design limit, provided that the current limits are not exceeded. The voltage and current waveforms in *abc* coordinates at the instant of closure S_1 are presented in Fig. 7. This figure shows that the variables are sinusoidal despite a large transient in the current required to synchronize the voltages of the microgrid to the host grid. Finally, following the closure of S_2 at $t = 1.5\,s$, the $\bar{\mathbf{u}}_k$ variables of all DER units revert to linear operation for both sets of boundaries, as can be seen in Fig. 8b. In this condition, all DER units track their respective output references, as shown in Fig. 6. Finally, some of the features of the dynamic behavior of the microgrid frequency during the transition to the grid-connected mode warrant comments. As the frequency is imposed by the main grid following

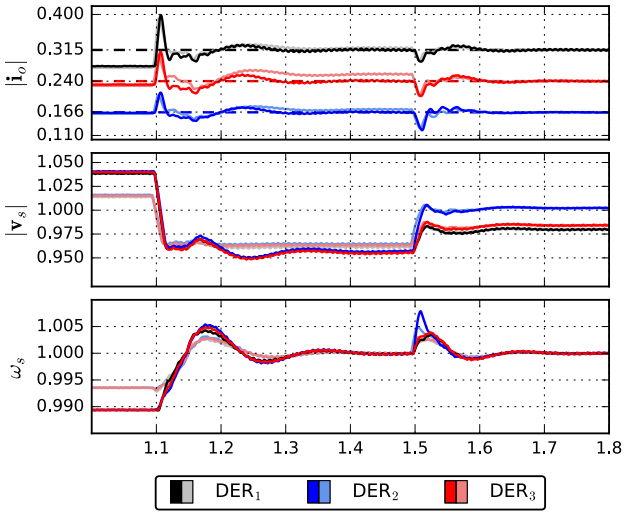

FIGURE 6. DER unit responses to the microgrid transition from islanded to grid-connected modes of operation. Response for input constraint $\mathbb{U}_1$ in dark-color lines and for input constraint $\mathbb{U}_2$ in light-color lines.

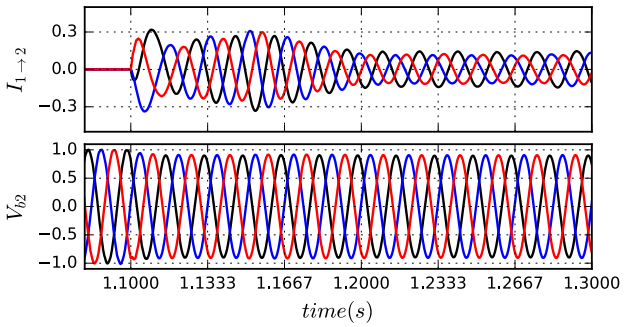

FIGURE 7. Current and voltage waveform for switch S_1.

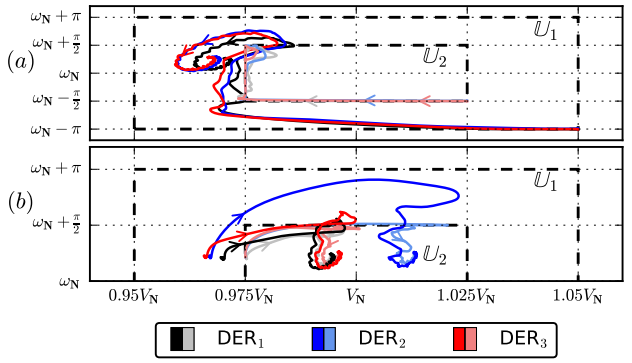

FIGURE 8. Trajectory of $\bar{\mathbf{u}}_k$ for transition to the grid-connected mode of operation. (a) Closure of switches S_1. (b) Closure of switch S_2. Responses for input constraint $\mathbb{U}_1$ in dark-color lines and for input constraint $\mathbb{U}_2$ in light-color lines.

TABLE 5. Experimental DER Systems Circuit and Control Parameters (v_N is the respective DER unit's nominal voltage and $\omega_N = 2\pi 50$ [rad/s]).

Circuit Parameters			
Par.	DER$_1$	DER$_2$	Units
R_f	90	100	$m\Omega$
L_f	5	5	mH
C_f	15	12	μF
R_g	327	327	$m\Omega$
L_g	594	594	μH
Input Constraints for $\bar{\mathbf{u}}_k$			
$\mathbb{U}$	$\mathbf{u}_\mathbf{s}^{\pm} = \begin{bmatrix} v_N(1\pm 0.025) & \omega_N \pm 0.5\pi \end{bmatrix}^T$		

TABLE 6. Closed-loop eigenvalues of the experimental DER units.

	$\lambda_{1,2}$		λ_3		$\lambda_{4,5}$		$\lambda_{6,7}$		λ_8	
	ω_n	ξ_n	ω_n	ξ_n	ω_n	ξ_n	ω_n	ξ_n	ω_n	ξ_n
DER$_1$	771	0.9	54	1	1522	0.6	1289	0.8	141	1
DER$_2$	806	0.9	67	1	1556	0.7	1320	0.8	141	1

the closure of S_1, the frequency component of the actuation term $\bar{u}_k^{(2)}$ (see equations (19) and (20)) is freed to drive the input to the new operating point, as is seen at the end of the trajectory in Fig. 8a or at the beginning in Fig 8b. Therefore, the overall frequency of the DER units exhibits an overshooting response that is characteristic of linear systems with double integration. In this case, the two integrations are embedded in the controller as well as the relationship between actuation ω_s and load angle δ.

V. EXPERIMENTAL RESULTS

The proposed control structure and design are experimentally validated in a simple laboratory microgrid consisting of two DER units connected to a three bus network, as shown in Fig. 9. Each DER unit is composed by a fixed 600 [V] DC source, a 5 [kVA] two-level VSC, and an *LC* output filter. The control of each DER unit is implemented in a separate DSpace 1103 platform, which sample the local variables and modulate the respective VSC with space-vector modulation at a frequency of 5 kHz. The nominal line-to-line voltage of DER$_1$ is 380 [V], whereas for DER$_2$ it is 220 [V]. Both DER units are connected to a 380 [V], 50 Hz network through respective isolation transformers. The transformer of DER$_1$ is connected through a 20 m long feeder to the common bus bar, whereas the transformer of DER$_2$ feeds directly to the common bus. The load and the switch to the main grid are located at the common bus bar. The parameters of the filters and transformers, and the voltage limits for the DER units are listed in Table 5. These values are used in the design of the proposed controller following the procedure described in Section III-C. The resulting closed-loop eigenvalues are reported in Table 6.

The first experimental result, depicted in Fig. 10, shows both DER units operating in the islanded mode (S_2 open) and independently (S_0 open). Initially, both DER units have zero current references, while S_1 is closed and, therefore, DER$_2$ feeds the resistive load (47Ω per-phase) with the voltage and frequency that are determined by the lower bound of the designed constraints. On the other hand,

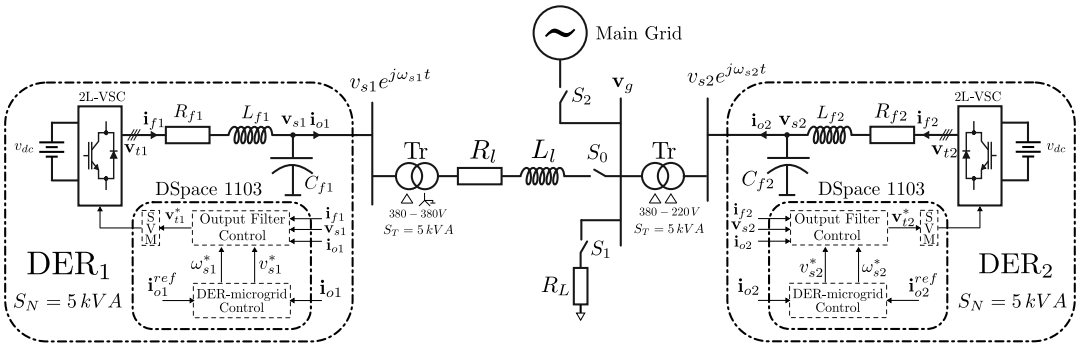

FIGURE 9. Unilineal diagram of the laboratory set-up for experimental validation.

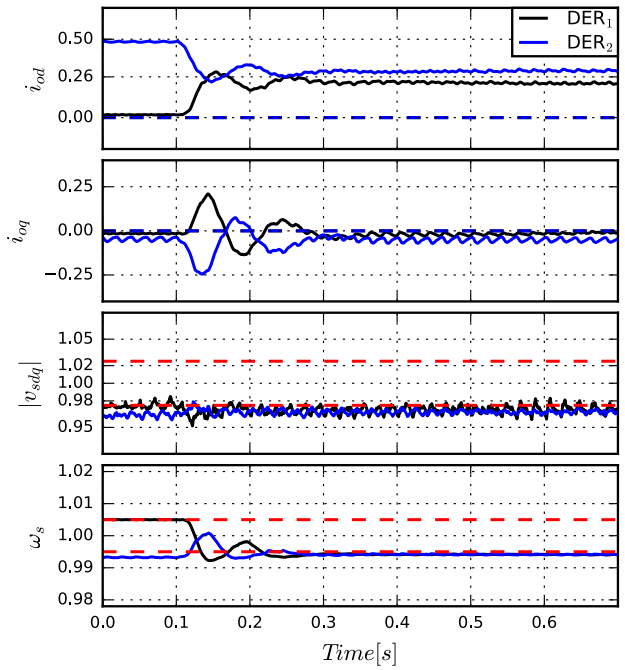

FIGURE 10. Experimental results in islanded mode. At $t = 0.1\,s$ the DER units are connected with a phase displacement of 5^o.

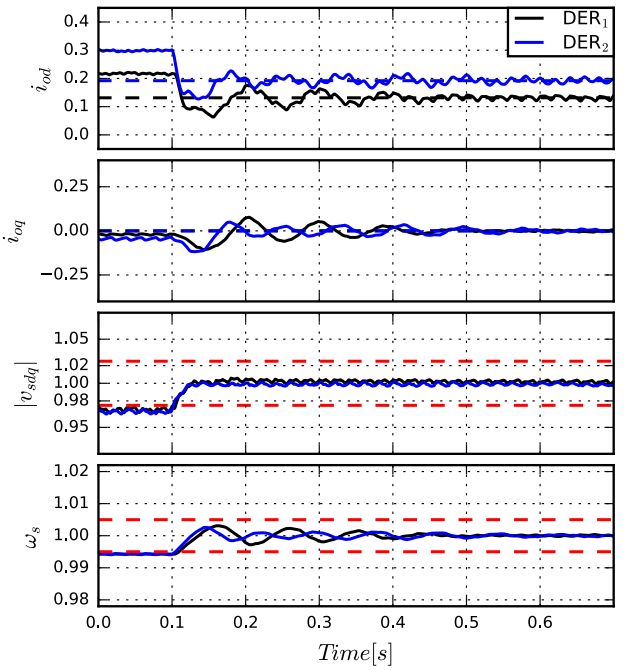

FIGURE 11. Experimental results of microgrid transition from islanded mode the grid-connected mode of operation. At $t = 0.1\,s$, S_2 is closed.

DER$_1$ is only loaded by its respective transformer and, consequently supplies mainly reactive current. This results in a voltage amplitude saturation at the lower bound, and voltage frequency saturation at the upper bound of the designed constraints. A small deviation from the designed constraint is observed, which is due the effect of the stabilizing feedback path of the proposed control. At $t = 0.1\,s$, S_0 is closed, while the voltages have a phase difference of approximately 5^o, connecting the two DER units in parallel. The initial phase difference excites the natural modes of the microgrid, but the modes are quickly damped and the DER units get synchronized and share the load. A small difference can be noticed in the loading of the DER units, which is due to the difference in the line impedances of the DER units.

The second set of experimental result is shown in Fig. 11. In this case, the DER units start operating in parallel in the islanded mode, with references $\mathbf{i}_{o1}^{ref} = 3+0j\,[A]$ and $\mathbf{i}_{o2}^{ref} = 4+0j\,[A]$. Due to the difference between the actual load and the references, the voltages are saturated at the lower bound of the designed constraints. At $t = 0.1\,s$, the microgrid is connected to the main grid, thus producing a transition from the islanded mode to the grid-connected mode of operation. Thereafter, the voltage amplitude and frequency are regulated by the main grid, allowing the DER units to track their respective output current references, as can be observed in Fig. 11.

VI. CONCLUSION

A single decentralized control law is proposed in this paper for inverter-based microgrids that must operate in both islanded and grid-connected modes of operation. The proposed control includes a model for uncertainties, which are estimated by an extended state observer. The estimated

uncertainties are compensated by an additive feedforward term which provides integral action to the controller. The integral action, in turn, provides steady-state current tracking at the possible cost of voltage amplitude and frequency deviations. Therefore, limits on voltage amplitude and frequency are imposed by partial input saturation. This combination of integral control and partial input saturation enables fully decentralized control of the inverters under various grid conditions, as well as seamless transitions between the two modes of operation. Furthermore, it is shown in this paper that the proposed control strategy preserves the stabilizing effect of the state feedback while it maintains the voltage amplitude and frequency regulation for the DER units within pre-specified limits.

Simulation results demonstrate the decentralized cooperation of the DER units for stabilizing the microgrid variables and reaching the closest feasible operating point with respect to their output current references. This includes current tracking when the microgrid's voltage allows it, as is the case in the grid-connected mode of operation; and seamless transition to voltage regulation when the grid condition does not permit it, as in the islanded mode of operation. Additionally, experimental results in a small laboratory microgrid confirm the practical feasibility of the proposed control technique.

REFERENCES

[1] Z. Li, M. Shahidehpour, F. Aminifar, A. Alabdulwahab, and Y. Al-Turki, "Networked microgrids for enhancing the power system resilience," *Proc. IEEE*, vol. 105, no. 7, pp. 1289–1310, Jul. 2017.

[2] D. E. Olivares, A. Mehrizi-Sani, A. H. Etemadi, C. A. Cañizares, R. Iravani, M. Kazerani, A. H. Hajimiragha, O. Gomis-Bellmunt, M. Saeedifard, R. Palma-Behnke, and G. A. Jiménez-Estévez, and N. D. Hatziargyriou, "Trends in microgrid control," *IEEE Trans. Smart Grid*, vol. 5, no. 4, pp. 1905–1919, Jul. 2014.

[3] A. Hirsch, Y. Parag, and J. Guerrero, "Microgrids: A review of technologies, key drivers, and outstanding issues," *Renew. Sustain. Energy Rev.*, vol. 90, pp. 402–411, Jul. 2018.

[4] J. Rocabert, A. Luna, F. Blaabjerg, and P. Rodríguez, "Control of power converters in AC microgrids," *IEEE Trans. Power Electron.*, vol. 27, no. 11, pp. 4734–4749, Nov. 2012.

[5] Y. Gu, N. Bottrell, and T. C. Green, "Reduced-order models for representing converters in power system studies," *IEEE Trans. Power Electron.*, vol. 33, no. 4, pp. 3644–3654, Apr. 2018.

[6] S. Sen and V. Kumar, "Microgrid control: A comprehensive survey," *Annu. Rev. Control*, vol. 45, pp. 118–151, Jan. 2018.

[7] F. Katiraei, M. R. Iravani, and P. W. Lehn, "Micro-grid autonomous operation during and subsequent to islanding process," *IEEE Trans. Power Del.*, vol. 20, no. 1, pp. 248–257, Jan. 2005.

[8] J. M. Guerrero, J. C. Vásquez, J. Matas, M. Castilla, and L. G. de Vicuña, "Control strategy for flexible microgrid based on parallel line-interactive UPS systems," *IEEE Trans. Ind. Electron.*, vol. 56, no. 3, pp. 726–736, Mar. 2009.

[9] C.-L. Chen, Y. Wang, J.-S. Lai, and Y.-S. Lee, "Design of parallel inverters for smooth mode transfer microgrid applications," *IEEE Trans. Power Electron.*, vol. 25, no. 1, pp. 6–15, Jan. 2010.

[10] Y. Mohamed and A. A. Radwan, "Hierarchical control system for robust microgrid operation and seamless mode transfer in active distribution systems," *IEEE Trans. Smart Grid*, vol. 2, no. 2, pp. 352–362, Jun. 2011.

[11] X. Li, H. Zhang, M. B. Shadmand, and R. S. Balog, "Model predictive control of a voltage-source inverter with seamless transition between islanded and grid-connected operations," *IEEE Trans. Ind. Electron.*, vol. 64, no. 10, pp. 7906–7918, Oct. 2017.

[12] Q. Cui, K. El-Arroudi, and G. Joós, "Islanding detection of hybrid distributed generation under reduced non-detection zone," *IEEE Trans. Smart Grid*, vol. 9, no. 5, pp. 5027–5037, Sep. 2018.

[13] D. Das, G. Gurrala, and U. J. Shenoy, "Linear quadratic regulator-based bumpless transfer in microgrids," *IEEE Trans. Smart Grid*, vol. 9, no. 1, pp. 416–425, Jan. 2018.

[14] M. C. Turner and D. J. Walker, "Linear quadratic bumpless transfer," *Automatica*, vol. 36, no. 8, pp. 1089–1101, 2000.

[15] M. Karimi-Ghartemani, S. A. Khajehoddin, P. Piya, and M. Ebrahimi, "Universal controller for three-phase inverters in a microgrid," *IEEE J. Emerg. Sel. Topics Power Electron.*, vol. 4, no. 4, pp. 1342–1353, Dec. 2016.

[16] U. Tamrakar, D. Shrestha, M. Maharjan, B. P. Bhattarai, T. M. Hansen, and R. Tonkoski, "Virtual inertia: Current trends and future directions," *Appl. Sci.*, vol. 7, no. 7, p. 654, 2017.

[17] B. Singh, G. Pathak, and B. K. Panigrahi, "Seamless transfer of renewable-based microgrid between utility grid and diesel generator," *IEEE Trans. Power Electron.*, vol. 33, no. 10, pp. 8427–8437, Oct. 2018.

[18] T. Shao, T. Q. Zheng, H. Li, and X. Zhang, "Parameter design and hot seamless transfer of single-phase synchronverter," *Electr. Power Syst. Res.*, vol. 160, pp. 63–70, Jul. 2018.

[19] M. B. Delghavi and A. Yazdani, "A unified control strategy for electronically interfaced distributed energy resources," *IEEE Trans. Power Del.*, vol. 27, no. 2, pp. 803–812, Apr. 2012.

[20] M. Fazeli and P. Holland, "Universal and seamless control of distributed resources-energy storage for all operational scenarios of microgrids," *IEEE Trans. Energy Convers.*, vol. 32, no. 3, pp. 963–973, Sep. 2017.

[21] N. Pogaku, M. Prodanovic, and T. C. Green, "Modeling, analysis and testing of autonomous operation of an inverter-based microgrid," *IEEE Trans. Power Electron.*, vol. 22, no. 2, pp. 613–625, Mar. 2007.

[22] R. Pérez-Ibacache, C. A. Silva, and A. Yazdani, "Linear state-feedback primary control for enhanced dynamic response of AC microgrids," *IEEE Trans. Smart Grid*, vol. 10, no. 3, pp. 3149–3161, May 2019.

[23] *Benchmark Systems for Network Integration of Renewable and Distributed Energy Resources*, CIGRE, Paris, France, 2014.

[24] N. Hatziargyriou, H. Asano, R. Iravani, and C. Marnay, "Microgrids," *IEEE Power Energy Mag.*, vol. 5, no. 4, pp. 78–94, Jul./Aug. 2007.

[25] C. K. Sao and P. W. Lehn, "Control and power management of converter fed microgrids," *IEEE Trans. Power Syst.*, vol. 23, no. 3, pp. 1088–1098, Aug. 2008.

[26] D. Pullaguram, S. Mishra, N. Senroy, and M. Mukherjee, "Design and tuning of robust fractional order controller for autonomous microgrid VSC system," *IEEE Trans. Ind. Appl.*, vol. 54, no. 1, pp. 91–101, Jan./Feb. 2018.

[27] H. Kwakernaak, *Linear Optimal Control Systems*. Hoboken, NJ, USA: Wiley, 1972, pp. 377–441.

[28] T. Söderström, *Discrete-Time Stochastic Systems: Estimation and Control*, 2nd ed. Secaucus, NJ, USA: Springer-Verlag, 2002, pp. 319–365.

[29] M. V. Kothare, P. J. Campo, M. Morari, and C. N. Nett, "A unified framework for the study of anti-windup designs," *Automatica*, vol. 30, no. 12, pp. 1869–1883, 1994.

[30] *IEEE Standard for Interconnection and Interoperability of Distributed Energy Resources With Associated Electric Power Systems Interfaces*, IEEE Standard 1547-2018 (Revision IEEE Std 1547-2003), Apr. 2018, pp. 1–138.

RICARDO PÉREZ-IBACACHE received the B.Eng. degree in electronic engineering from Universidad Técnica Federico Santa María, Valparaíso, Chile, and the M.Sc.Eng. and Dr.Eng. degrees in electronic engineering from Universidad Técnica Federico Santa María, Valparaíso, in 2012 and 2018, respectively. He is currently a Postdoctoral Researcher (CAPES) with the Grupo de Automação e Controle de Sistemas, PUCRS, Porto Alegre, Brazil. His main research interests include power electronics, primary control of microgrids, and robust control design.

AMIRNASER YAZDANI (M'05–SM'09) received the Ph.D. degree in electrical engineering from the University of Toronto, Toronto, ON, Canada, in 2005. He was an Assistant Professor with the University of Western Ontario (UWO), London, ON, Canada. He is currently a Professor with Ryerson University, Toronto. His research interests include modeling and control of electronic power converters, renewable electric power systems, distributed generation and storage, and microgrids. He is the Lead Coauthor of the book *Voltage-Sourced Converters in Power Systems* (IEEE-Wiley Press, 2010). He is also an Associate Editor of the IEEE TRANSACTIONS ON SUSTAINABLE ENERGY.

CÉSAR SILVA (S'01–M'02) received the B.Eng. degree in electronic engineering from Universidad Técnica Federico Santa María (UTFSM), Valparaíso, Chile, in 1998, and the Ph.D. degree from the University of Nottingham, U.K., in 2003. In 1999, he joined as a Postgraduate Research Student at the Power Electronics Machines and Control Group, University of Nottingham, U.K., where he was granted the Overseas Research Students Awards Scheme. In 2002, he joined the Departamento de Electrónica, UTFSM, Chile, where he is currently an Associate Professor. He teaches electric machines theory, power electronics, and ac machine drives. His main research interests include sensorless vector control of ac machines drives and digital control of static converters in different applications, including microgrids.

JUAN C. AGÜERO was born in Osorno, Chile. He received the M.Eng. degree from Universidad Técnica Federico Santa María, Chile, in 2000, and the Ph.D. degree from The University of Newcastle, Australia, in 2006. He gained industrial experience in the copper mining industry at El Teniente, Codelco, Chile, from 1997 to 1998. He was a Research Academic with The University of Newcastle, Australia, in 2014. He is currently a Professor Adjunto with Universidad Técnica Federico Santa María, Chile, where he received the professional title of Ingeniero Civil Electrónico. His research interests include system identification and control and statistical signal processing.